THE JOURNAL OF PHYSICAL CHEMISTRY B

Article

pubs.acs.org/JPCB

Structures and Surface Tensions of Fluids near Solid Surfaces: An Integral Equation Theory Study

Mengjin Xu,[†] Chen Zhang,[†] Zhongjie Du,*[,†] and Jianguo Mi*[,‡]

[†]The Key Laboratory of Carbon Fiber and Functional Polymers, Ministry of Education, Beijing University of Chemical Technology, Beijing 100029, People's Republic of China

[‡]State Key Laboratory of Organic−Inorganic Composites, Beijing University of Chemical Technology, Beijing 100029, China

ABSTRACT: In this work, integral equation theory is extended to describe the structures and surface tensions of confined fluids. To improve the accuracy of the equation, a bridge function based on the fundamental measure theory is introduced. The density profiles of the confined Lennard-Jones fluids and water are calculated, which are in good agreement with simulation data. On the basis of these density profiles, the grand potentials are then calculated using the density functional approach, and the corresponding surface tensions are predicted, which reproduce the simulation data well. In particular, the contact angles of water in contact with both hydrophilic and hydrophobic walls are evaluated.

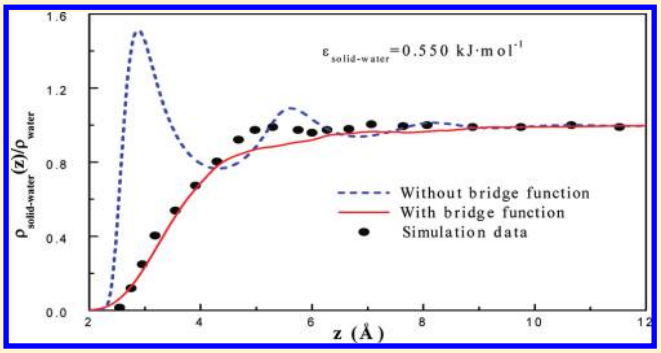

1. INTRODUCTION

The study of fluid adsorbed on solid substrates continues to be a subject of great interest since the structure of fluid at the interface is thought to determine their wetting properties. In recent decades, numerous computational and theoretical studies have been devoted to it. Computer simulation has proven to be a powerful tool for understanding the microscopic mechanisms of wetting.[1−7] Meanwhile, statistical mechanical theories provide a flexible and high-efficient way to deal with it.[8−10]

Of various theoretical approaches, classical density functional theory (DFT) has been successfully applied to adsorption, wetting, layering transition, and capillary condensation at planar and nonplanar substrates.[11,12] The key issue of DFT is to derive an expression for the grand potential. By minimizing the grand potential, the structure of fluid near a solid substrate can be determined, and the surface energy distribution as well as the surface tension can be easily obtained. The priority of DFT over mean field theory is attributed to its accurate energy calculation. However, most investigations merely concern model fluids at simple interfaces. The theory, when extended to real fluids, such as water, electrolytes, or polymers, is no longer suitable because an analytical free energy functional for dipole, associating, electrostatic, or intramolecular interactions is quite difficult to construct. Although the widely used statistical associating fluid theory provides a practical way for these complicated fluids,[13] the semiempirical methodology cannot describe the detailed structure of the confined systems. Moreover, some potential parameters have to be regressed from experimental data. Recently, a relatively rigorous DFT approach proposed by Jain et al.[14−16] has been extended to associating and chain fluids. Given the complexity of the free energy functional, its reliability and efficiency need to be further examined. On the other hand, it is quite difficult to derive an analytical free energy functional formula for fluid in contact with a rough surface.[17−19]

Compared with DFT, Ornstein−Zernike (OZ) integral equation theory (IET) describes the structure of bulk and inhomogeneous fluids directly through different correlation functions, where different intra- or intermolecular interactions can be easily involved. Given a suitable description of intra- and intermolecular interactions and an accurate closure equation, IET can provide satisfactory radial distribution function (RDF) of bulk fluids even without the introduction of bridge function. For example, the RDF of water can be accurately calculated by the equation using the hypernetted chain (HNC) approximation and the renormalized technique of electrostatic potentials.[20] More importantly, the further developed three-dimensional IET allows a reliable description of the structure of real fluids in contact with a rough surface.[21,22] However, IET cannot provide accurate free energy expression and has been qualified as a relatively weak field method.[23] It is well-known that the primary source of inaccuracy is due to the uncertainty of the bridge function, which can be expressed as an infinite sum of highly connected bridge diagrams.[23] Because of its complicated form, the function is usually neglected in many approximate solutions. This deficiency is inevitably exaggerated when extended to solid−fluid interfaces.

The effect of the bridge function in IET has been extensively investigated in several decades. Much work has focused on

Received: February 29, 2012
Revised: May 10, 2012
Published: May 11, 2012

   dx.doi.org/10.1021/jp301991k | J. Phys. Chem. B 2012, 116, 6514−6521

heuristic, semiempirical methodologies. All such approaches, which include the Verlet approximation,[24] the Martynov–Sarkisov approximation,[25,26] and the Duh–Haymet–Henderson approximation[27,28] as well as many others,[29,30] have shown improvement over the HNC closure for real systems. The accuracy of such results, however, is far from satisfaction for inhomogeneous system. Meanwhile, an approach to deduce the bridge function from the fundamental measures functional[31] has been developed by Rosenfeld[32] and has been applied to various fluids.[33] Its efficiency has been demonstrated in high asymmetric and confined systems.[34−36]

Another deficiency of IET is that it cannot calculate the free energy directly. It is well-known that the direct correlation function (DCF) derived from the OZ equation is inaccurate for hard-sphere reference system; thus, the resulting DCF cannot be used for energy calculation. Such a puzzle may be solved if the density functional approach is integrated. In the process of constructing the bridge function, the free energy functional for hard-sphere reference is also calculated. Given the quantitatively accurate density profile and the improved DCF, the whole free energy functional can be constructed through the modified fundamental measure theory[37] and the perturbation expansion method.

In this work, we propose an integral equation route to investigate the density profiles and surface tensions of Lennard-Jones (LJ) fluids and water near solid surfaces. This work is motivated by the need for an accurate theoretical model that can treat real solid–water interfaces. Similarly to the previous study,[31−36] we apply the fundamental measure theory[31] to construct the bridge function, and we insert it into the OZ equation. The fluid density profiles for different systems are initially calculated, and the free energy functional is then predicted by the modified fundamental measure theory for hard sphere and by the perturbation theory for attractive contribution. The essential task of the present work is to develop a reliable approach to quantitatively calculate the structures and thermodynamic properties of confined real fluids.

2. THEORY AND EQUATIONS

The structure of multisite fluid such as water can be directly described by the OZ equation, which can be generally expressed as[38]

$$h_{ij}(r) = \sum_k \int d\mathbf{r}' \omega_{ik}(\mathbf{r} - \mathbf{r}') \sum_\lambda \int d\mathbf{r}'' c_{k\lambda}(\mathbf{r}' - \mathbf{r}'') [\omega_{\lambda j}(r'') + \rho_\lambda h_{\lambda j}(r'')] \quad (1)$$

where the subscripts i, j, k, and λ represent interaction sites in a fluid molecule. h is the total correlation function, c is the DCF, and ρ_λ is the density of site λ. $\omega(r)$ is the intramolecular correlation function with the form

$$\omega_{ik}(r) = \frac{\delta(r - l_{ik})}{4\pi l_{ik}^2} \quad (2)$$

where l_{ik} is the intramolecular distance between i and k, and δ stands for Dirac delta function. For the confined fluid, eq 1 becomes

$$h_{Sj}(r) = \sum_i \int d\mathbf{r}' c_{Si}(\mathbf{r}')[\omega_{ij}(\mathbf{r} - \mathbf{r}') + \rho_i h_{ij}(\mathbf{r} - \mathbf{r}')] \quad (3)$$

where the subscript S means the solid surface, which can be nanoparticle or planar wall. For the LJ fluid, the intramolecular correlation function no longer exists, and eqs 1 and 3 can be simplified. The closure equation employed here has the form

$$h_{ij}(r) = \exp[-\beta u_{ij}(r) + h_{ij}(r) - c_{ij}(r) + b_{ij}(r)] - 1 \quad (4)$$

where u is the interaction potential and b is the bridge function.

The bridge function can be derived from the fundamental measure theory. The molecular force field of water is described by the SPC/E model.[39] In the model, the H site is treated as simple point charge without volume and mass; thus, the bridge functions relating to H site (such as b_{HH}, b_{OH}, and b_{SH}) are set to be zero. Meanwhile, b_{OO} can be calculated with the same method as that for the simple LJ fluid, and b_{SO} is the same as that for the confined LJ fluid. According to the fundamental measure theory, the bridge function can be computed from[36]

$$b_{ii}(\mathbf{r}) = -\beta(\mu_i^{ex,hs}(\mathbf{r}) - \mu_i^{ex,hs}(\rho_i)) - \rho_i \int d\mathbf{r}' c_{ii}^{hs}(\mathbf{r}') h_{ii}(\mathbf{r} - \mathbf{r}') \quad (5)$$

for homogeneous fluid and from

$$b_{Si}(\mathbf{r}) = -\beta(\mu_i^{ex,hs}(\mathbf{r}) - \mu_i^{ex,hs}(\rho_i)) - \rho_i \int d\mathbf{r}' c_{ii}^{hs}(\mathbf{r}') h_{Si}(\mathbf{r} - \mathbf{r}') \quad (6)$$

for the fluid in contact with a solid surface. $c^{hs}(\mathbf{r})$ is the hard-sphere DCF, and $\mu^{ex,hs}(\rho_i)$ is the excess chemical potential of the hard sphere for the bulk fluid. $\mu^{ex,hs}(\mathbf{r})$ is the local excess chemical potential functional of the hard sphere, which can be given by

$$\beta\mu^{ex,hs}(\mathbf{r}) = \int d\mathbf{r}' \sum_\alpha \mu_\alpha[n_\alpha(\mathbf{r}'); \mathbf{r}']\varpi^{(\alpha)}(\mathbf{r} - \mathbf{r}') \quad (7)$$

Here, $n_\alpha(\mathbf{r})$ and $\varpi^{(\alpha)}(\mathbf{r})$, α = 0, 1, 2, 3, V1, V2, are the weighted densities and the weight functions, respectively. $n_\alpha(\mathbf{r})$ is defined as

$$n_\alpha(\mathbf{r}) = \int \rho(\mathbf{r}')\varpi^{(\alpha)}(\mathbf{r} - \mathbf{r}')d\mathbf{r}' \quad (8)$$

and $\varpi^{(\alpha)}(\mathbf{r})$ is expressed in terms of the Heaviside step function $H(r)$ and the Dirac delta function $\delta(r)$ with

$$\varpi^{(2)}(\mathbf{r}) = \pi\sigma^2\varpi^{(0)}(\mathbf{r}) = 2\pi\sigma\varpi^{(1)}(\mathbf{r}) = \delta(\sigma/2 - r) \quad (9)$$

$$\varpi^{(3)}(\mathbf{r}) = H(\sigma/2 - r) \quad (10)$$

$$\varpi^{(V2)}(\mathbf{r}) = 2\pi\sigma\varpi^{(V1)}(\mathbf{r}) = \frac{\mathbf{r}}{r}\delta(\sigma/2 - r) \quad (11)$$

The function $c^{hs}(\mathbf{r})$ in eqs 5 and 6 can be computed as the second functional derivatives of Φ

$$-c^{hs}(\mathbf{r}) = \sum_{\alpha,\gamma} \left[\frac{\partial^2\Phi}{\partial n_\alpha \partial n_\gamma}\right]_{\{n_{\alpha,0}\}} \int d\mathbf{r}'\varpi^{(\alpha)}(\mathbf{r}')\varpi^{(\gamma)}(\mathbf{r} - \mathbf{r}') \quad (12)$$

and $\mu_\alpha[n_\alpha(\mathbf{r})]$ in eq 7 can be derived from the excess free energy density Φ for hard-sphere reference

$$\mu_\alpha[\{n_\alpha(\mathbf{r})\}] = \frac{\partial\Phi}{\partial n_\alpha} \quad (13)$$

dx.doi.org/10.1021/jp301991k | J. Phys. Chem. B 2012, 116, 6514−6521

The free-energy density of hard-sphere reference system is given by the modified fundamental measure theory[37] including both the scalar and vector contributions

$$\Phi(\mathbf{r}) = \left[-n_0 \ln(1-n_3) + \frac{n_1 n_2 - \mathbf{n}_{V1}\cdot\mathbf{n}_{V2}}{1-n_3} + \frac{1}{36\pi}\left(n_3 \ln(1-n_3) + \frac{n_3^2}{(1-n_3)^2}\right)\frac{n_2^3 - 3n_2\mathbf{n}_{V2}\cdot\mathbf{n}_{V2}}{n_3^3}\right] \quad (14)$$

Once the equilibrium density distribution of the fluid near a solid surface is obtained, the grand potential $\Omega[\rho(\mathbf{r})]$, or equivalently the intrinsic Helmholtz free energy, can be calculated with

$$\Omega[\rho(\mathbf{r})] = \int d\mathbf{r}\rho(\mathbf{r})[\ln(\rho(\mathbf{r})\Lambda^3) - 1] + F^{rep}[\rho(\mathbf{r})] + F^{att}[\rho(\mathbf{r})] + \int d\mathbf{r}[\rho(\mathbf{r})(V^{ext}(\mathbf{r}) - \mu_b)] \quad (15)$$

where Λ is the thermal de Broglie wavelength, $F^{rep}[\rho(\mathbf{r})]$ is the Helmholtz free energy for hard-sphere repulsion, $F^{att}[\rho(\mathbf{r})]$ is the attractive contribution, and $V^{ext}(\mathbf{r})$ is the solid−fluid potential. For hard-sphere repulsion

$$F^{rep}[\rho(\mathbf{r})] = k_B T \int \Phi(\mathbf{r})d\mathbf{r} \quad (16)$$

For the attractive interaction, $F^{att}[\rho(\mathbf{r})]$ can be written as

$$F^{att}[\rho(\mathbf{r})] = F^{att}[\rho_b] + \mu_b^{att}\int d\mathbf{r}\Delta\rho(\mathbf{r}) - \frac{1}{2}\int d\mathbf{r}\Delta\rho(\mathbf{r})\int d\mathbf{r}_1\Delta\rho(\mathbf{r}_1)c_b^{att}(\mathbf{r}-\mathbf{r}_1) \quad (17)$$

for fluid near a planar wall and as

$$F^{att}[\rho(\mathbf{r})] = F^{att}[\rho_b] + \mu_b^{att}\int \frac{\mathbf{r}_1}{\mathbf{r}}d\mathbf{r}_1\Delta\rho(\mathbf{r}_1) - \frac{1}{2}\int \frac{\mathbf{r}_1}{\mathbf{r}}d\mathbf{r}_1\Delta\rho(\mathbf{r}_1)\int \frac{\mathbf{r}_2}{\mathbf{r}_1}d\mathbf{r}_2\Delta\rho(\mathbf{r}_2)c_b^{att}(\mathbf{r}_1-\mathbf{r}_2) \quad (18)$$

for fluid near a spherical nanoparticle. Here, $\Delta\rho(\mathbf{r}) = \rho(\mathbf{r}) - \rho_b$. $c_b^{att}(r)$ is the attractive part of the bulk DCF. It is defined as the difference between the total DCF $c(r)$ and the hard-sphere DCF $c^{hs}(r)$

$$c_b^{att}(r) = c(r) - c^{hs}(r) \quad (19)$$

Once the accurate RDF or $g(r)$ is obtained, the total Helmholtz free energy of the bulk fluid can be easily calculated by

$$a = \ln(\rho_b\Lambda^3) - 1 + \frac{4\eta - 3\eta^2}{(1-\eta)^2} + 2\pi\beta\rho_b\int_0^\infty g(r)u(r)r^2dr \quad (20)$$

in which η is the packing fraction of bulk fluid with $\eta = \pi/6\rho\sigma^3$. The corresponding chemical potential μ_b can be derived from the free energy $\mu_b = \partial(\rho_b a)/\partial\rho_b$. With the obtained density profile, the surface tension γ_s can be calculated by

$$\gamma_S = \int_0^\infty [f[\rho(z)] - \rho(z)a + \rho(z)V^{ext}(z) + Z[\rho - \rho(z)]]dz \quad (21)$$

for planar surface and by

$$\gamma_S = \int_R^\infty \left(\frac{r}{R}\right)^2 [f[\rho(r)] - \rho(r)a + \rho(r)V^{ext}(r) + Z[\rho - \rho(r)]]dr \quad (22)$$

for curved surface. In eqs 21 and 22, f is the Helmholtz free energy density, and Z is the compression factor.

According to the theoretical framework, $h(r)$ for the bulk LJ fluid or $h_{OO}(r)$, $h_{OH}(r)$, and $h_{HH}(r)$ for water need to be first calculated. $h(r)$ or $h_{OO}(r)$ is then applied to construct the corresponding bridge function. $h_{OO}(r)$, $h_{OH}(r)$, and $h_{HH}(r)$ can be accurately calculated by a renormalized technique.[20]

3. RESULTS AND DISCUSSION

Theory provides a simple and flexible way to obtain structure and properties of confined fluids in a short time. However, its predictive applicability has to be tested in order to find the scope of application. When dealing with a specific solid−fluid system, an effective way to test theory is to compare its calculation results with molecular simulation data, which can in principle represent exactly the behavior of a system. Therefore, the calculated density profiles are compared with the corresponding simulation data.

3.1. Test with Molecular Simulation. Figure 1 presents the density profile of the LJ fluid in contact with a hard wall.

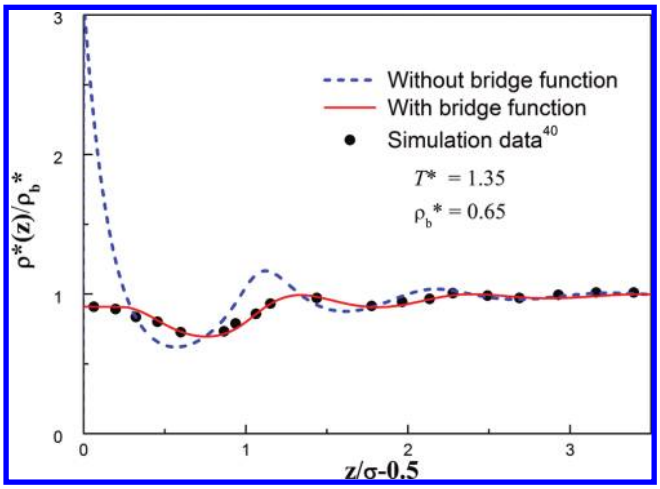

Figure 1. Density profile of the LJ fluid in contact with a hard wall (the wall is located at $z/\sigma = 0$).

The reduced density of the fluid is $\rho^* = 0.65$, and the reduced temperature is $T^* = 1.35$. It shows that, with $b(r)$ correction, the OZ equation successfully accounts for the depletion around the solid−fluid interface, and its performance is quantitatively satisfactory when compared with the simulation data.[40] In contrast, the equation without consideration of $b(r)$ is not only quantitatively unreliable but also qualitatively questionable. It fails to represent the depletion, and the density oscillation cannot be sufficiently suppressed. Once $b(r)$ is omitted, the inconsistency between $c(r)$ and $h(r)$ is greatly exaggerated for this asymmetrical system. As a result, $b(r)$ has greatly modified the self-consistency of the integral equation.

dx.doi.org/10.1021/jp301991k | J. Phys. Chem. B 2012, 116, 6514−6521

Another typical instance is the LJ fluid near hard spherical particles with varying size. The introduced external potential is

$$V^{\mathrm{ext}}(\mathbf{r}) = \begin{cases} \infty, & r/\sigma < D \\ 0, & r/\sigma > D \end{cases} \tag{23}$$

in which D defined as $D = (\sigma_n/\sigma + 1)/2$ is the shortest dimensionless distance between the particle and a fluid molecule. σ_n and σ are the diameters of the particle and the LJ fluid, respectively. The reduced density of the fluid is $\rho^* = 0.70$, and the reduced temperature is $T^* = 0.85$. The inhomogeneous system exhibits an interesting phenomenon that resembles the solvophobic effects. Figure 2 shows that, if

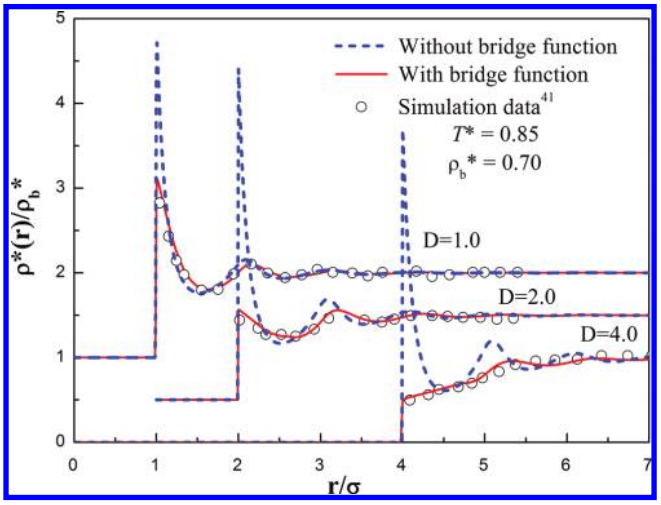

Figure 2. Density profiles of the LJ fluid around nanoparticles with different sizes. To enhance visual clarity, the profiles of $D = 1$ and 2 are shifted upward by 1.0 and 0.5, respectively.

the particle size is close to the LJ fluid, the density profile is highly oscillatory and very much likes the RDF of the LJ fluid. As the particle size increases, however, the oscillation rapidly decreases, and a drying layer with a vaporlike density is formed around the particle surface. If the particle is large enough, the recovery from the drying layer to the bulk density can be essentially monotonous. To a large extent, this behavior is similar to that of LJ molecules around hard walls. If $b(r)$ is added, the equation is able to account for the transition from solvophilicity to solvophobicity. The agreement between the theory and computer simulation[41] is quite good. In contrast, the density profiles without $b(r)$ correction are highly oscillatory in all cases, and their first peaks always occur at the contact. Therefore, it is conclusive that, once the bridge function is neglected, the OZ equation is incapable of showing depletion around hard walls or hard spheres. The introduction of the bridge function leads to a significant improvement in description of the density profiles both at planar and curved surfaces.

3.2. Lennard-Jones Fluid near Solid Surface. In the following discussions, we adopt the Lennard-Jones/spline potential to describe the fluid−fluid and solid−fluid interactions

$$u_{ij}^{\mathrm{LJS}}(r, s) = \begin{cases} 4\varepsilon_{ij}\left[\left(\frac{\sigma_f}{r-s}\right)^{12} - \left(\frac{\sigma_f}{r-s}\right)^{6}\right], & 0 < r-s < r_{s,ij} \\ a_{ij}(r-s-r_{c,ij})^2 + b_{ij}(r-s-r_{c,ij})^3, & r_{s,ij} < r-s < r_{c,ij} \\ 0, & r_{c,ij} < r-s \end{cases} \tag{24}$$

where r is the distance, σ_f is the diameter of the fluid molecule, ε_{ij} is the potential depth for interaction between species i and j, and $s = (\sigma_n - \sigma_f)/2$, where $\sigma_n = 2R$ is the diameter of the nanoparticle. The remaining variables are given by $r_{s,ij} = (26/7)^{1/6}\sigma_f$, $r_{c,ij} = (67/48)r_{s,ij}$, $a_{ij} = -(24\,192/3211)(\varepsilon_{ij}/r_{s,ij}^2)$, and $b_{ij} = -(387\,072/61\,009)(\varepsilon_{ij}/r_{s,ij}^3)$. Consequently, $u_{ff}^{\mathrm{LJS}}(r, 0)$ indicates the fluid−fluid potential, and $u_{nf}^{\mathrm{LJS}}(r, s)$ denotes the nanoparticle−fluid interaction. If $s \to \infty$, the potential changes to $u_{wf}^{\mathrm{LJS}}(r, s)$ representing the wall−fluid interaction. $u_{nf}^{\mathrm{LJS}}(r, s)$ and $u_{wf}^{\mathrm{LJS}}(r, s)$ are served as the external potential $V_{\mathrm{ext}}(r)$. Since the potential has been applied in the molecular simulation[1] to study the surface tensions, it is convenient to examine our theoretical predictions.

Figure 3 summarizes the density profiles of an LJ fluid near solid walls with different wall−fluid interaction strengths. The

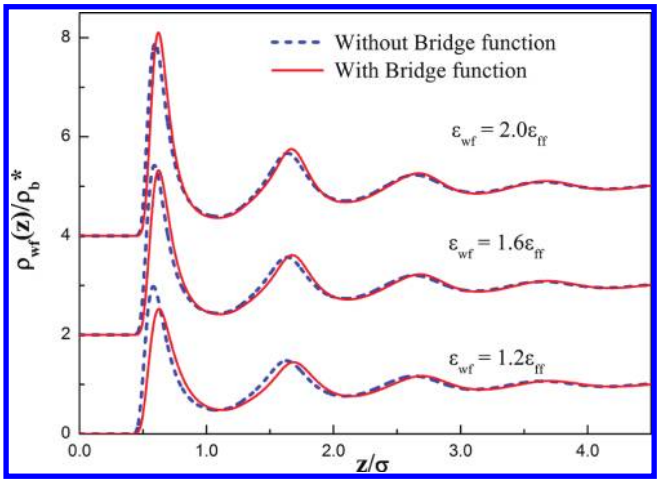

Figure 3. Density profiles of the LJ fluid at planar surfaces with different interactions. (The wall is located at $z/\sigma = 0$, and the profiles for $\varepsilon_{wf} = 1.6\varepsilon_{ff}$ and $2.0\varepsilon_{ff}$ are shifted upward by 2 and 4, respectively.)

pVT properties of the bulk fluid are $\rho^* = 0.675$, $T^* = 0.75$, and $p^* = 0.026$. The density profile depends strongly on the interaction strength ε_{wf}. Especially, the local density defined by the first adsorption layer shows an obvious decrease as the strength decreases. According to Bresme and Quirke,[1] at high interaction strength with $\varepsilon_{wf} = 2.0\varepsilon_{ff}$, the wall exhibits solvophilic effect; if the strength decreases to $\varepsilon_{wf} = 1.2\varepsilon_{ff}$, the wall then exhibits solvophobic effect. Comparing the density profiles with and without consideration of $b(r)$, one can see that $b(r)$ has improved the first peaks at $\varepsilon_{wf} = 2.0\varepsilon_{ff}$ representing a positive contribution to density fluctuation. Instead, if the interaction strength decreases to $\varepsilon_{wf} = 1.6\varepsilon_{ff}$, $b(r)$ changes to suppress the local density of the first adsorption layer indicating a negative contribution to density fluctuation. The effect becomes more obvious at $\varepsilon_{wf} = 1.2\varepsilon_{ff}$.

dx.doi.org/10.1021/jp301991k | J. Phys. Chem. B 2012, 116, 6514−6521

The calculated bridge functions for wall−fluid system are plotted versus the interaction strengths in Figure 4. Obviously,

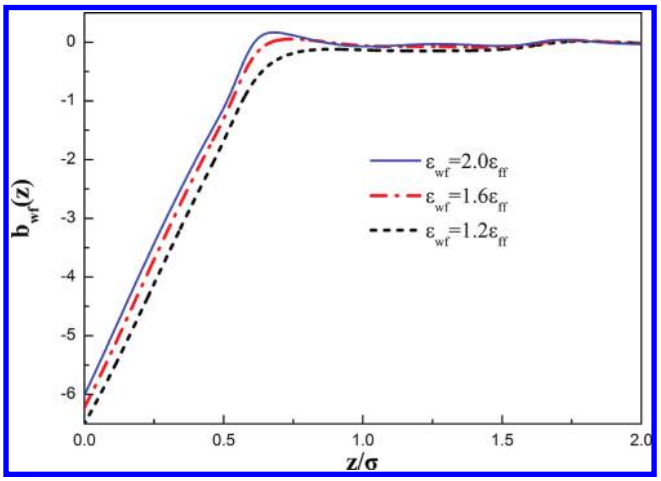

Figure 4. Bridge functions between the LJ fluid and the planar surfaces with different interactions. (The wall is located at $z/\sigma = 0$.)

$b(r)$ is dependent on the wall−fluid interaction strength. At high strength, $b(r)$ contains both positive and negative values; upon decreasing the interaction strength, the whole $b(r)$ becomes entirely negative. Another important function is the DCF between wall and fluid. As shown in Figure 5, at high

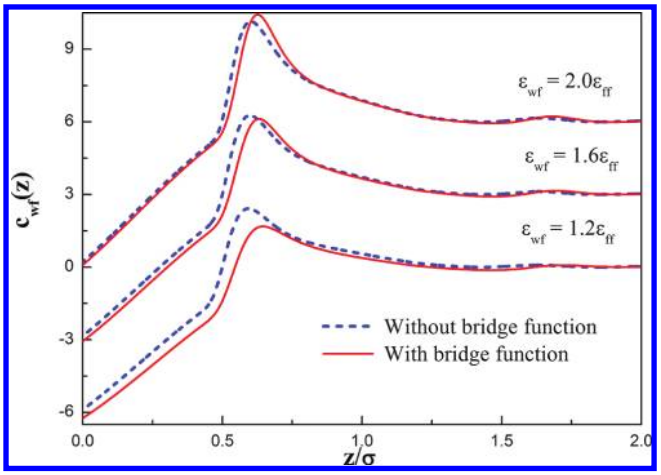

Figure 5. DCFs between the LJ fluid and the planar surfaces with different interactions. (The wall is located at $z/\sigma = 0$, and the functions for $\varepsilon_{wf} = 1.6\varepsilon_{ff}$ and $2.0\varepsilon_{ff}$ are shifted upward by 3 and 6, respectively.)

strength with $\varepsilon_{wf} = 2.0\varepsilon_{ff}$, $b(r)$ improves the peak of DCF, which represents the main part of attractive contribution. As the wall−fluid interaction strength decreases, the depletion effect increases, and $b(r)$ decreases the attractive contribution. Combining Figures 3−5, we can conclude that the first peak of the density profile decreases as the attractive part of the DCF decreases and the bridge function becomes more negative.

In addition to the planar surface, we have analyzed a simple curved surface, where the same LJ fluid around different nanoparticles is considered. The density profiles are depicted in Figure 6 for one representative interaction strength $\varepsilon_{nf} = 1.25\varepsilon_{ff}$. The corresponding bridge functions and DCFs for nanoparticle−fluid interactions are shown in Figures 7 and 8, respectively. The local density defined by the first adsorption

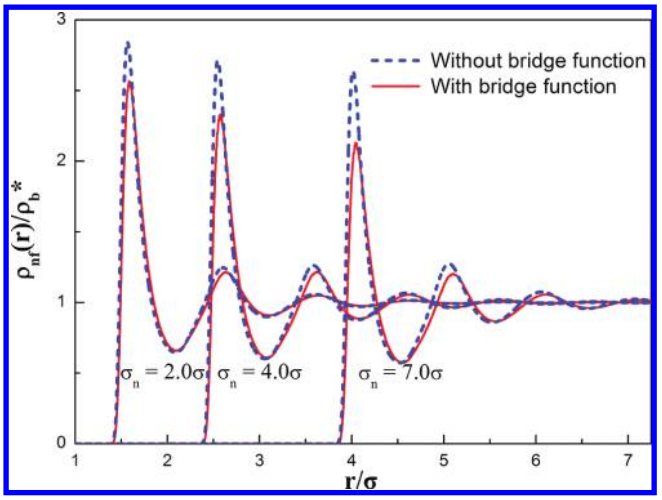

Figure 6. Density profiles of the LJ fluid around nanoparticles with different sizes.

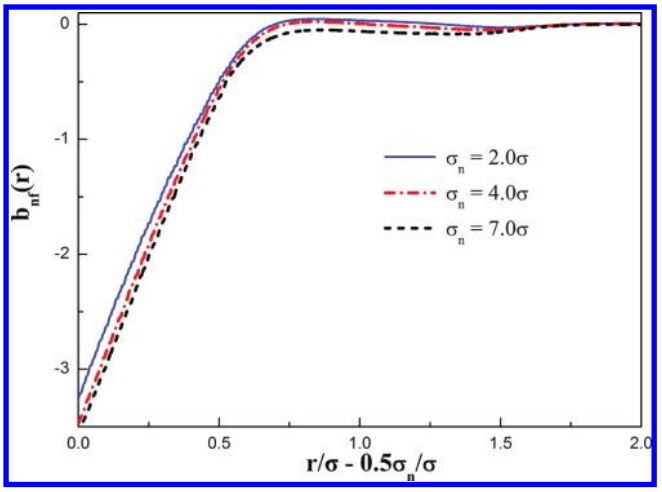

Figure 7. Bridge functions between the LJ fluid and nanoparticles with different sizes.

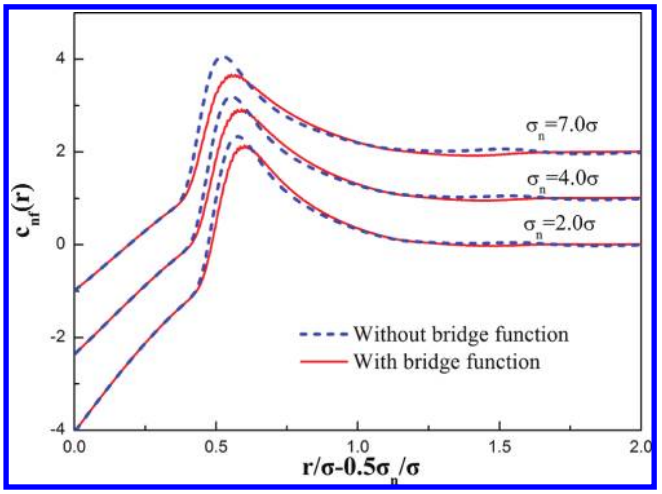

Figure 8. DCFs between the LJ fluid and nanoparticles with different sizes (the functions for $\sigma_n = 4.0\sigma$ and 7.0σ are shifted upward by 1 and 2, respectively).

layer shows a decreasing tendency with the increasing of particle size. Meanwhile, the effect of $b(r)$ on density profile

dx.doi.org/10.1021/jp301991k | J. Phys. Chem. B 2012, 116, 6514−6521

increases as the particle size increases. The accuracy of density profiles can be evaluated through surface tension calculation, which will be discussed below. In Figure 8, the attractive part of the DCFs has been suppressed through the introduction of $b(r)$, and the effect of $b(r)$ also increases as the particle size increases. As for $b(r)$ itself, although no simulation data are available with which to compare, the current results show a similar behavior as those derived from the density expansion method.[42]

With the density profile, the grand potential of the interfacial fluid is calculated. In addition, the excess Helmholtz free energy of the bulk fluid is calculated though its RDF using the perturbation theory approach. The surface tensions are accordingly predicted. In Figure 9, we present the surface tensions of an LJ fluid near different solid walls, and we compare these results with the simulation data,[1] where $\varepsilon_{wf}/\varepsilon_{ff}$ = 2.2 and $\varepsilon_{wf}/\varepsilon_{ff}$ = 1.0 correspond to complete wetting and drying,[1] respectively. The agreement is excellent except for complete wetting or drying. The failure of the certain OZ equation to account for complete wetting or drying has been analyzed by Evans et al.[43] In Figure 10, the nanoparticle−liquid surface tensions as a function of the particle size are plotted. It also shows a good reproduction of the simulation data for the small particle−fluid systems (the size is smaller than 5σ) and for the wall−fluid system (a wall can be viewed as a special sphere of infinite diameter). As for large particle and fluid systems, the simulation data show irregular fluctuation, while our theoretical calculations give a smooth curve. Summarizing Figures 9 and 10, we can draw a conclusion that the present approach is reliable to predict the surface tensions of planar and spherical interfaces for the LJ fluid from solvophilic to solvophobic cases.

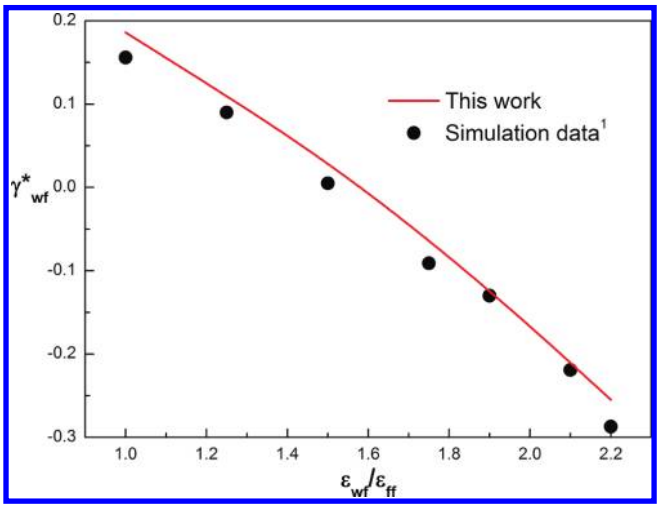

Figure 9. Wall−fluid surface tensions as a function of wall−fluid interaction strength.

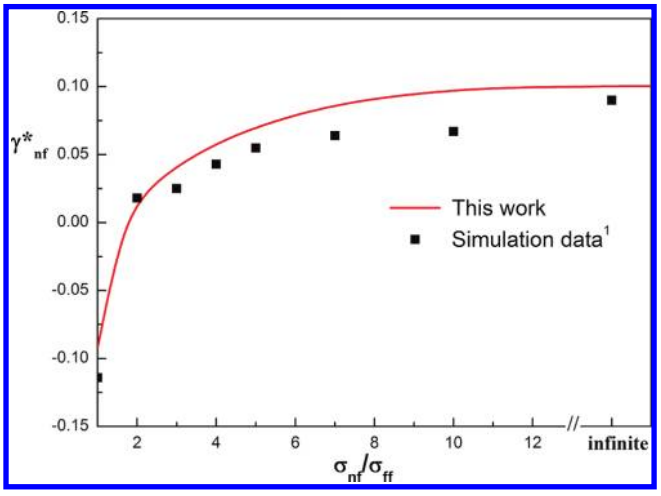

Figure 10. Nanoparticle−fluid surface tensions as a function of particle size.

3.3. Water near Solid Surface. Compared with LJ fluid, water has more complicated structure and properties. A water molecule has three sites, and both the LJ and the associating interactions exist between any two molecules. These interactions are included in the SPC/E model. If water is in contact with a neutral solid, because of the absence of mass/size/LJ interaction of hydrogen in the SPC/E model, all of the LJ interactions are carried by the water oxygen atom; thus, the solid−water interactions can be described by

$$u_{SO}(z) = 2\pi\sigma_O^2\varepsilon_{SO}\left[\frac{2}{5}\left(\frac{\sigma_O}{z}\right)^{10} - \left(\frac{\sigma_O}{z}\right)^4\right] \quad (25)$$

where ε_{SO} is the potential between water and solid surface.

Figure 11 shows the density profile of liquid water in contact with a hydrophilic wall at T = 300 K. The calculated distribution curve displays a sharp peak near 3.5 Å, a dip near 5.0 Å, and a second peak around 6.0 Å. Compared with the simulation data, the integrated equation with the bridge function correction yields a relatively lower adsorption in the first layer. If the bridge function is not considered, the equation gives a much higher adsorption. Obviously, the bridge function makes the equation more accurate in the region of the first peak.

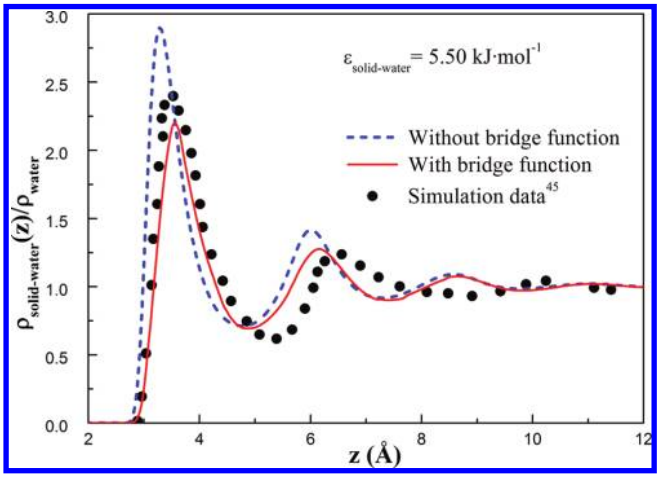

Figure 11. Density profile of water over the hydrophilic surface.

The effect of the bridge function is more obvious for liquid water in contact with a hydrophobic wall at T = 300 K. As shown in Figure 12, the calculated density profile is similar to the simulation data, which displays a relatively simple behavior. Around 6 Å from the surface, the density gradually increases to the bulk value. However, the equation without the bridge function produces an artificial peak. Figure 12 shows clearly that, with the consideration of the bridge function, the

dx.doi.org/10.1021/jp301991k | J. Phys. Chem. B 2012, 116, 6514−6521

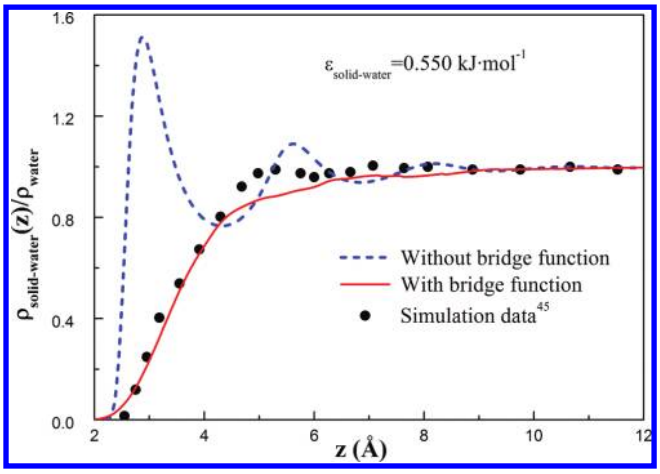

Figure 12. Density profile of water over the hydrophobic surface.

exaggerated adsorption in the first layer is successfully corrected.

Given the density profiles of the liquid water in contact with different solid surfaces, the surface tensions are calculated using eqs 15−21. At the hydrophilic surface, the calculated surface tensions are -2.5×10^{-3} and -19.8×10^{-3} N/m with and without the bridge function correction. At the hydrophobic surface, the corresponding values are 66.8×10^{-3} and 29.4×10^{-3} N/m, respectively. To compare with the simulation data, the corresponding surface tensions of equilibrium water vapor in contact with the solid surfaces are also calculated with the same method. For vapor water, the density is very low leading to the surface tension being overlooked. In addition, the vapor−liquid interfacial tension of water is taken directly from the experimental value,[44] which is 71.7×10^{-3} N/m. Thus, the contact angles can be approximately determined by Young's equation. The final predictive results are 88° and 74° on the hydrophilic surface with and without the bridge function correction, and the results are 159° and 114° on the hydrophobic surface with and without the bridge function correction. In molecular simulation,[45] the contact angles of water near the two surfaces were measured directly, which are 84° and 156° on the hydrophilic and hydrophobic surfaces, respectively. It is shown that, without the bridge function, the OZ equation cannot predict correct contact angle for hydrophobic interface, and the deviation for hydrophilic interface is also obvious; once the bridge function is integrated, the equation can produce more reasonable results under hydrophilic and hydrophobic conditions.

For the above water−solid systems, although only the LJ interaction exists between oxygen and solid, the three-site structure and the point charge of hydrogen are taken fully into account for both homogeneous and inhomogenous water. The information has been integrated into the bridge function. In this regard, the present method can be extended to more complicated systems with multisite interactions between fluid and solid.

4. CONCLUSION

In summary, a modified integral equation approach has been used to describe the density profiles and surface tensions of the confined LJ fluid and water in which the bridge function deduced from Rosenfeld's fundamental measures functional is integrated. For LJ fluid, the accuracy of density distributions has been extensively improved at planar and curved interfaces. The calculated surface tensions are also in good agreement with the simulation data indicating that the interface free energy calculation is reliable. In particular, the present approach provides a rigorously theoretical model to investigate the properties of water in contact with hydrophilic and hydrophobic surfaces. Good agreement between theory and simulation shows that the present approach is quantitatively reasonable for a confined water system. Since the approach contains the advantages of both the integral equation and the density functional approach, it would be helpful to analyze more complicated systems.

AUTHOR INFORMATION

Corresponding Author

*E-mail: duzj@mail.buct.edu.cn (Z.D.); mijg@mail.buct.edu.cn (J.M.).

Notes

The authors declare no competing financial interest.

ACKNOWLEDGMENTS

This work is supported by the Program for New Century Excellent Talents in University, and the financial support of the National Natural Science Foundation of China (Nos. 21076006) is also greatly appreciated.

REFERENCES

(1) Bresme, F.; Quirke, N. *J. Chem. Phys.* **1999**, *110*, 3536−3547.
(2) Moody, M. P.; Attard, P. *J. Chem. Phys.* **2001**, *115*, 8967−8977.
(3) Tay, K. A.; Bresme, F. *J. Am. Chem. Soc.* **2006**, *128*, 14166−14175.
(4) Domínguez, A.; Oettel, M.; Dietrich, S. *J. Chem. Phys.* **2008**, *128*, 114904.
(5) Bresme, F.; Lehle, H.; Oettel, M. *J. Chem. Phys.* **2009**, *130*, 214711.
(6) Horsch, M.; Heitzig, M.; Dan, C.; Harting, J.; Hasse, H.; Vrabec, J. *Langmuir* **2010**, *26*, 10913−10917.
(7) Kumar, V.; Sridhar, S.; Errington, J. R. *J. Chem. Phys.* **2011**, *135*, 184702.
(8) Fischer, J.; Methfessel, M. *Phys. Rev. A* **1980**, *22*, 2836−2843.
(9) Evans, R.; Henderson, J. R.; Roth, R. *J. Chem. Phys.* **2004**, *121*, 12074−12084.
(10) Zeng, M; Mi, J.; Zhong, C. *Phys. Chem. Chem. Phys.* **2011**, *13*, 3932−3941.
(11) Davis, H. T. *Statistical Mechanics of Phases, Interfaces and Thin Films*; Wiley-VCH: Weinheim, Germany, 1996.
(12) Rowlinson, J. S.; Widom, B. *Molecular Theory of Capillarity*; Oxford University Press: Oxford, United Kingdom, 1989.
(13) Fu, D.; Li, X. S. *J. Chem. Phys.* **2006**, *125*, 084716.
(14) Jain, S.; Dominik, A.; Chapman, W. G. *J. Chem. Phys.* **2007**, *127*, 244904.
(15) Bymaster, A.; Dominik, A.; Chapman, W. G. *J. Phys. Chem.C* **2007**, *111*, 15823−15831.
(16) Bymaster, A.; Chapman, W. G. *J. Phys. Chem. B* **2010**, *114*, 12298−12307.
(17) Bryk, P.; Rżysko, W.; Malijevsky, A.; Sokołowski, S. *J. Colloid Interface Sci.* **2007**, *313*, 41−52.
(18) Henderson, D.; Sokołowski, S.; Wasan, D. *Phys. Rev. E* **1998**, *57*, 5539−5543.
(19) Bryk, P.; Henderson, D.; Sokołowski, S. *Langmuir* **1999**, *15*, 6026−6034.
(20) Xu, Q.; Mi, J.; Zhong, C. *J. Chem. Phys.* **2010**, *133*, 174104.
(21) Kovalenko, A.; Hirata, F. *Chem. Phys. Lett.* **1998**, *290*, 237−244.
(22) Ratkova, E. L.; Chuev, G. N.; Sergiievskyi, V. P.; Fedorov, M. V. *J. Phys. Chem. B* **2010**, *114*, 12068−12079.
(23) Zhou, Y.; Stell, G. *J. Stat. Phys.* **1988**, *52*, 1389−1412.
(24) Verlet, L. *Mol. Phys.* **1980**, *41*, 183−190.

(25) Martynov, G. A.; Sarkisov, G. N. *Mol. Phys.* **1983**, *49*, 1495−1504.
(26) Ballone, P.; Pastore, G.; Galli, G.; Gazzillo, D. *Mol. Phys.* **1986**, *59*, 275−290.
(27) Duh, D. M.; Haymet, A. D. J. *J. Chem. Phys.* **1992**, *97*, 7716−7729.
(28) Duh, D. M.; Henderson, D. *J. Chem. Phys.* **1996**, *104*, 6742−6754.
(29) Perkyns, J.; Pettitt, B. M. *Theor. Chem. Acc.* **1997**, *96*, 61−70.
(30) Dyer, K.; Perkyns, J.; Pettitt, B. M. *J. Chem. Phys.* **2002**, *116*, 9413−9421.
(31) Rosenfeld, Y. *Phys. Rev. Lett.* **1989**, *63*, 980−983.
(32) Rosenfeld, Y. *J. Chem. Phys.* **1993**, *98*, 8126−8148.
(33) Kahl, G.; Bildstein, B.; Rosenfeld, Y. *Phys. Rev. E* **1996**, *54*, 5391−5406.
(34) Ayadim, A.; Malherbe, J. G.; Amokrane, S. *J. Chem. Phys.* **2005**, *122*, 234908.
(35) Amokrane, S.; Ayadim, A.; Malherbe, J. G. *J. Phys. Chem. C* **2007**, *111*, 15982−15988.
(36) Ayadim, A.; Amokrane, S. *J. Phys. Chem. B* **2010**, *114*, 16824−16831.
(37) Yu, Y.; Wu, J. *J. Chem. Phys.* **2002**, *117*, 10156−10164.
(38) Chandler, D.; Andersen, H. C. *J. Chem. Phys.* **1972**, *57*, 1930−1937.
(39) Berendsen, H. J. C.; Grigera, J. R.; Straatsma, T. P. *J. Phys. Chem.* **1987**, *91*, 6269−6271.
(40) Balabanic, C.; Borstnik, B.; Milcic, R.; Rubcic, A.; Sokolic, F. *Static and Dynamic Properties of Liquids*; Springer: Berlin, 1989.
(41) Huang, D. M.; Chandler, D. *Phys. Rev. E* **2000**, *61*, 1501−1506.
(42) Chen, W. W.; Huang, H. C.; Kwak, S. K. *Mol. Phys.* **2010**, *108*, 1531−1537.
(43) Evans, R.; Tarazona, P.; Marconi, U. M. B. *Mol. Phys.* **1983**, *50*, 993−1011.
(44) Nguyen, N. T.; Wereley, S. T. *Fundamentals and Applications of Microfluidics*; Artech House: London, 2006.
(45) Trudeau, T. G.; Jena, K. C.; Hore, D. K. *J. Phys. Chem. C* **2009**, *113*, 20002−20008.